Sensors & Actuators: A. Physical 344 (2022) 113739

Contents lists available at ScienceDirect

Sensors and Actuators: A. Physical

journal homepage: www.journals.elsevier.com/sensors-and-actuators-a-physical

Capacitive eye tracker made of fractured carbon nanotube-paper composites for wearable applications

Vigneshwar Sakthivelpathi [a], Zhongjie Qian [a], Tianyi Li [a], Sanggyeun Ahn [b], Anthony B. Dichiara [c], Robijanto Soetedjo [d], Jae-Hyun Chung [a,*]

[a] Department of Mechanical Engineering, University of Washington, Box 352600, Seattle, WA 98195, USA
[b] Department of Industrial Design, University of Washington, Seattle, WA 98195, USA
[c] School of Environment and Forest Sciences, University of Washington, Seattle, WA 98195, USA
[d] Department of Physiology and Biophysics, University of Washington, Box 357290, Seattle, WA 98195, USA

ARTICLE INFO

Keywords:
Capacitive sensor
Carbon nanotube paper composites
Eye tracking
Wearable
Human-machine interface

ABSTRACT

The uniqueness of eyes, facial geometry, and gaze direction makes eye tracking a very challenging technological pursuit. Although camera-based eye-tracking systems are popular, the obtrusiveness of their bulky equipment along with their high computational cost and power consumption is considered problematic for wearable applications. Noncontact gaze monitoring using capacitive sensing technique has been attempted but failed due to low sensitivity and parasitic capacitance. Here, we study the interaction between a novel capacitive sensor and eye movement for wearable eye-tracking. The capacitive sensors are made of a pair of asymmetric electrodes; one comprising carbon nanotube-paper composite fibers (CPC) and the other being a rectangular metal electrode. The interaction between the asymmetric sensor and a spherical object mimicking an eyeball is analyzed numerically. Using a face simulator, both single- and differential capacitive measurements are characterized with respect to proximity, geometry, and human body charge. Using a prototype eye tracker, multiple sensor locations are studied to determine the optimal configurations. The capacitive responses to vertical and horizontal gaze directions are analyzed in comparison to those of a commercial eye tracking system. The performance is demonstrated for sensitive eye-movement tracking, closed-eye monitoring, and human-machine interface. This research has important implications for the development of capacitive, wearable eye trackers, which can facilitate fields of human-machine interface, cognitive monitoring, neuroscience research, and rehabilitation.

1. Introduction

Since naked-eye observation in 1879, eye movement has been investigated for diagnosing neurological disorders [1,2], sleeping disorders [3,4], and learning disabilities [5,6]. For example, deficits in making saccades to a memorized location and suppressing a planned-saccade are potentially associated with intellectual disability, epilepsy, cerebellar ataxia [7], and other disorders related to metabolic diseases [8,9]. Abnormal saccades are also associated with several neurological disorders, including Creutzfeldt-Jakob disease [10], autism [11], Parkinson's disease [12], and Huntington's disease [13].

A study of the oculomotor system correlates eye movements with neuronal activity in different areas of the brain [14–16]. To accurately describe this relationship, an eye-tracking sensor needs to capture both spatial and temporal characteristics of eye movement with high fidelity [17]. With current oculomotor research turning to optogenetics [18,19], light is used to manipulate the activity of specific neurons with high temporal resolution. The real-time characteristics of an eye-tracking device are essential to describe the effects of an optical excitation on eye movement [20].

The gold standard for oculomotor research has been the scleral search coil system [21–23]. The scleral search coil system has the advantage of real-time, low-latency electronics, low noise, and high accuracy ($< 0.1°$) [24]. Currently, camera-based eye-tracking systems are the major workhorse for commercial applications. Due to the high demands for power and computational resources, current wearable eye trackers are tethered to a battery and a high-performance processor.

To address the challenges, other methods have been attempted.

Abbreviations: CPC, Carbon nanotube paper composite; PR, Paired rectangular; PF, Paired fibrous; PH, Paired hybrid.

* Corresponding author.
E-mail address: jae71@uw.edu (J.-H. Chung).

https://doi.org/10.1016/j.sna.2022.113739
Received 17 May 2022; Received in revised form 26 June 2022; Accepted 6 July 2022
Available online 8 July 2022

When eyes move, the polarization of the retina can be measured with electrooculography (EOG) [25,26]. Graphene electrodes have been used to improve the electrical interface to the skin [27]. Another eye-tracking technique measures the voltage generated by a piezoelectric nano-generator attached to the eyelid [28,29]. In contrast to the contact methods, a capacitive sensor has the potential to determine eye gaze direction without contact [30]. The movement of eyeballs, muscles, and eyelids induces a capacitive change with respect to a fixed point near the eyeball [31]. However, traditional capacitive sensors have not been able to produce accurate eye tracking.

In this paper, we present a wearable capacitive sensor made of a pair of asymmetric electrodes; one is carbon nanotube paper composite (CPC) fibers, and the other is a rectangular metal electrode. CPC is chosen as the electrode material because the high aspect ratio of the CPC fibrous structure increases the surface area and fringing capacitance, improving sensitivity. The CPC fibers are fabricated by a wet-fracture method, which allows for flexibility and miniaturization suitable for wearable eye trackers The capacitive interaction between asymmetric electrodes and a spherical eyeball is analyzed by numerical study. Using a face simulator, both single- and differential capacitive measurements are characterized to correlate eyeball movement and capacitive changes in terms of proximity, geometry, and human body charge. Based on the interaction study, multiple sensor locations are explored to find the optimal sensor locations for tracking the human eyeball. Vertical and

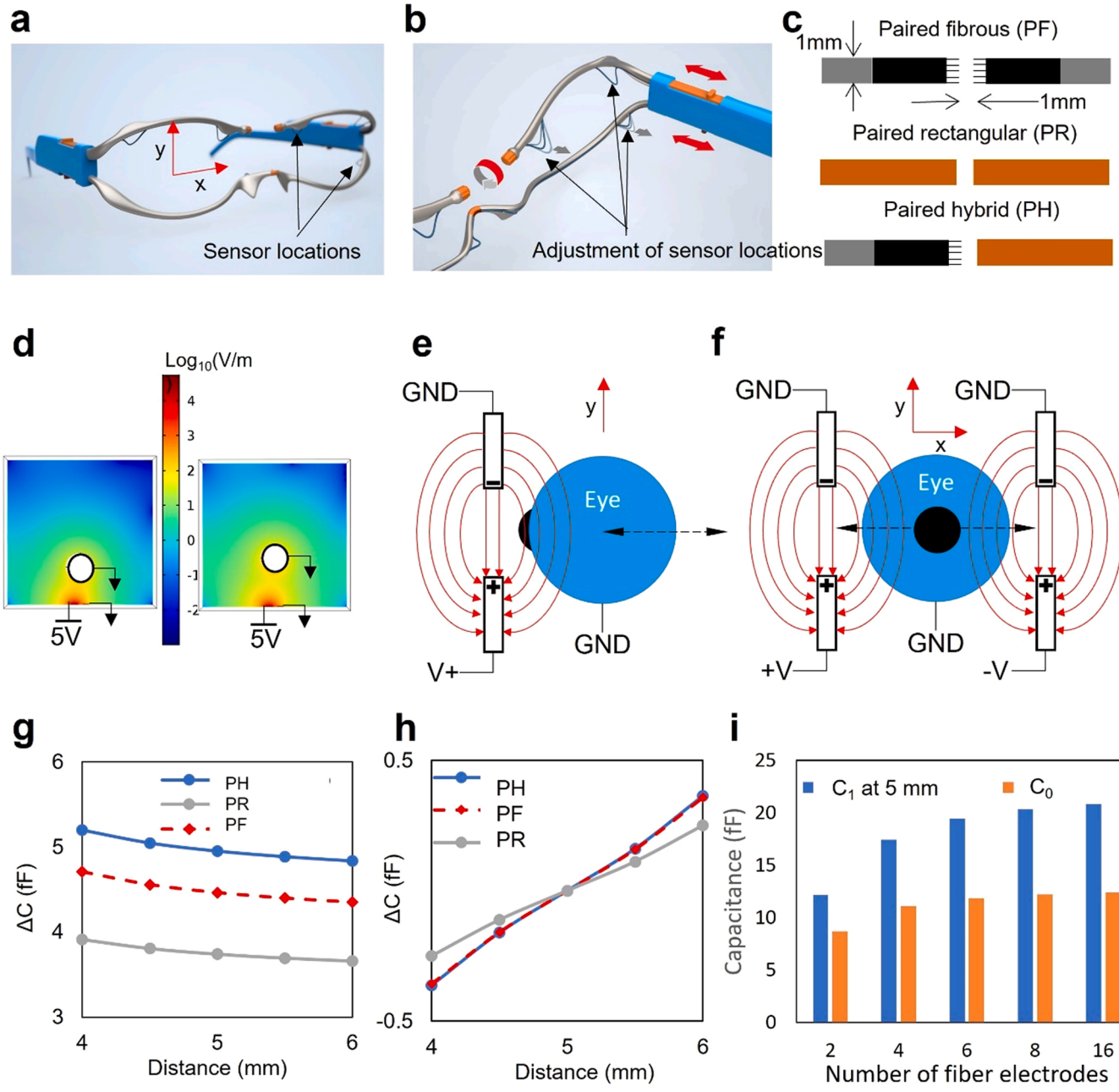

Fig. 1. Capacitance-based eye tracker. (a) Prototype design of an eye tracker. **(b)** Adjustment of sensor distance to the human eyeball. **(c)** The tested capacitive sensors consist of paired fibrous (PF), paired rectangular (PR), and paired hybrid (PH) electrodes. **(d)** Electric field distribution with a spherical object at 4 and 6 mm distances from a PH sensor. **(e)** Single capacitance measurement. **(f)** Differential capacitance measurement. **(g)** Numerical model of ΔC of PF, PR, and RH capacitances for the distance between 4 and 6 mm to a target sphere. **(h)** Numerical model of ΔC of differential measurement using PF, PR, and PH sensors. 5 mm is set as 0 fF for differential sensing. **(i)** Numerical model of initial (C_0) and working (C_1) capacitances of a PH sensor depending on the number of fibers. C_1 refers to the capacitance with the spherical target at 5 mm and C_0 is the capacitance without target.

horizontal eye movements are compared to those produced by a commercial eye tracker. The prototype eye tracker is demonstrated for smooth-pursuit eye-movement tracking, human-machine interface, and closed-eye movement monitoring.

2. Capacitive eye tracker

A wearable eye tracker that we envision is an eyeglass frame with integrated capacitive sensors (Fig. 1a). The miniaturized sensors allow for integration into existing headgears, such as virtual reality (VR) headsets. To fit individual face shapes, malleable mounts are used to adjust the sensor location and distance (Fig. 1b). Fig. 1c shows the geometry of the designed sensor that has 1×5 mm^2 area with 0.1 mm thickness. For capacitive measurement, the asymmetry in the geometrical shape of the eyeball near the scleral-corneal junction causes the distance change of the eyeball surface to the sensor under rotation. The distance change affects the fringing electric field, which in turn changes the capacitance.

Three different electrode combinations were analyzed for sensitivity evaluation by numerical computation. One was paired fibrous (PF) electrodes, another was paired rectangular (PR) electrodes, and the last one was paired hybrid (PH) electrodes consisting of fibrous and rectangular electrodes. The capacitive sensitivity was the ratio of capacitance change to distance change ($\Delta C/\Delta d$), where C was the capacitance and d was the distance between a sensor and an eyeball. A numerical model was built for the three sensor configurations with an eyeball. The rectangular metal electrode was 40×10 μm^2 in cross-section and 1 mm in length. The fibrous electrode was composed of four fibers having 10×10 μm^2 in cross-section and 1 mm in length. A detailed view of the numerical model is given in Fig. S1 (Supporting Information). The gap size was 1 mm. A 5 mm-diameter sphere, representing an eyeball, floats in the center (Fig. 1d). A 5 V AC potential with 25 kHz frequency is applied between the two electrodes. For hybrid electrodes, 5 V is applied to the fiber electrode while the rectangular metal electrode is grounded. The relative permittivity of a spherical object is 80.

The ΔC due to the fringing electric field could be computed by either single (Fig. 1e) or differential methods (Fig. 1f). The single method was convenient but suffered from the nonlinear relationship between capacitance and rotation angle. The differential method applied AC voltage 180° out of phase to the second sensor. The differential method doubled the sensitivity, canceled the nonlinearity, and, therefore, produced better linearity between capacitance and rotation angle. The advantage of differential measurement is mathematically described the Taylor's series expansion (Supporting Information, Sensitivity analysis for single and differential sensor configuration).

The numerical study indicates that, as the distance between the sphere and the sensor decreased from 6 to 4 mm, the charge interaction increased significantly between the eyeball and the positive electrode (Fig. 1d). Without the eyeball, the initial capacitance (C_0) of PR, PH, and PF sensors increased sequentially due to the increased surface area of the electrodes (Supporting Information, Fig. S2). When the eyeball was moved from 4 to 6 mm with 0.5 mm intervals, the ΔC increased gradually. Among the three sensor configurations, PH electrodes showed the highest ΔC followed by those of PF and PR electrodes in our numerical results (Fig. 1g). When the differential measurement was applied on ΔC, the sensitivity was further increased with better linearity (Fig. 1h).

PH electrodes showed the highest ΔC due to the reduced C_0 without an eyeball and the larger C_1 (capacitance with the spherical target at 5 mm) with an eyeball. The larger ΔC resulted in the enhanced sensitivity. The PH sensor was composed of a fibrous CPC electrode mated to a rectangular metal electrode. The fractured CPC generated conductive, high aspect ratio fibers at the end of electrode, which led to larger electric field strength and surface area in comparison to traditional plate electrodes. Due to the larger surface area, C_0 without an object increased in the following order: PR, PH, and PF electrodes. When a charged object like an eyeball was present, the fibrous electrodes of PH and PF showed a higher capacitance (C_1). As a result, the sensitivity ($\Delta C/\Delta d$) of the PH sensor, which combined rectangular and fibrous electrodes, outperformed the PR and PF sensors.

The C_0, C_1, and ΔC saturated as the number of fibers increased for a hybrid capacitance (Fig. 1i). ΔC saturated when the number was greater than 8. Despite the random fiber shapes, the aspect ratio (length/width) greater 100 and the fiber number greater than 8 could offer uniform ΔC values due to the saturation.

3. Material and methods

3.1. Fabrication of fibrous electrodes

A capacitive sensor was made of carbon nanotube-paper composites (CPC) using the previously reported methods [32,33]. The fabricated CPC had a mean thickness of 88.4 ± 3.1 μm. For sensor fabrication, the initial material was cut into 1×10 mm^2 (Fig. 2a). After patterning silver (MG Chemicals, 8330S-21 G, USA) electrodes on both ends of the material, a 0.1 mm capillary pen was used to print a water line at the center of the material. With the water line soaking CPC fibers, tensional fracture was induced to separate the material. Through the wet-stretching process, two 1×5 mm^2 fibrous electrodes were fabricated. For rectangular electrodes, silver ink (Engineered Materials Systems, Inc. Cl-1001, NY) was uniformly coated on a polyethylene terephthalate (PET) film. A silver-coated PET film was trimmed to 1×10 mm^2. By combining fibrous and rectangular electrodes, three kinds of electrode pairs were fabricated; PF, PH, and PR electrodes (Fig. 2a). A 50 μm-thick self-adhesive polyethylene terephthalate (PET) film was used for laminating the capacitive sensors. The fabricated PF, PH, and PR sensors are shown in Fig. 2b. The gap between electrodes was 1 mm. For fibrous electrodes, the gap size was the distance between the final ends of PF electrodes. For PH electrodes, the gap size was the distance from the end of the fibers and the square edge of the rectangular electrode. For the PR electrode the gap size was the distance between the square edges. The detailed fabrication process is provided in the Supporting Information (Fig. S4). When C_0 values were compared for PR, PF, and PH electrodes, the average values were 321.0 ± 2.6 fF, 373.0 ± 13.2 fF, and 360.7 ± 7.7 fF, respectively ($N = 3$, Supporting Information, Fig. S5). The ratio of the standard deviation to the average was 0.8%, 3.5%, and 2.1% for PR, PF, and PH electrodes, respectively. Although the morphology was not the same, the variation in the measured capacitance of PF electrodes remained within 3.5%, which resulted in consistent sensitivity across the fabricated sensors. The sequential increase of C_0 values for PR, PH, and PF electrodes agreed with the sequence of the numerical modeling results (Supporting Information, Fig. S6).

According to scanning electron microscope (SEM) study, the average thickness of fibers was 5.9 ± 1.6 μm (Fig. 2c). The aspect ratio determining the electric field strength ranged from 200 to 490. The linear density of fibers was 14.5 ± 3.6 mm^{-1}. The X-ray diffraction (XRD) profiles (Supporting Information, Fig. S7), collected with a Bruker D8 Discover system equipped with a high-efficiency Cu (1.54 Å) anode, showed that CNTs were uniformly dispersed in the CPC matrix, which is crucial for predictable capacitance of the cantilevered fibers [34–36].

3.1.1. Measurement circuit

Two kinds of capacitance-to-digital converters (CDC) were used to measure capacitance, AD7747 (Analog Devices) and FDC1004 (Texas Instruments). An AD7747 chipset was used for single- or differential measurement of capacitance. It was powered by a 3.3 V input, enabling a 16 kHz excitation output and 45 Hz sampling rate. Although an AD7747 offered a high accuracy capacitance measurement (0.1 aF), the chip could measure only two capacitance channels.

An FDC1004 chip was used to construct the eye tracker circuit for benchmarking against the Tobii Pro Nano. FDC1004 was powered by a 3.3 V input. The excitation frequency was 25 kHz with a measurement

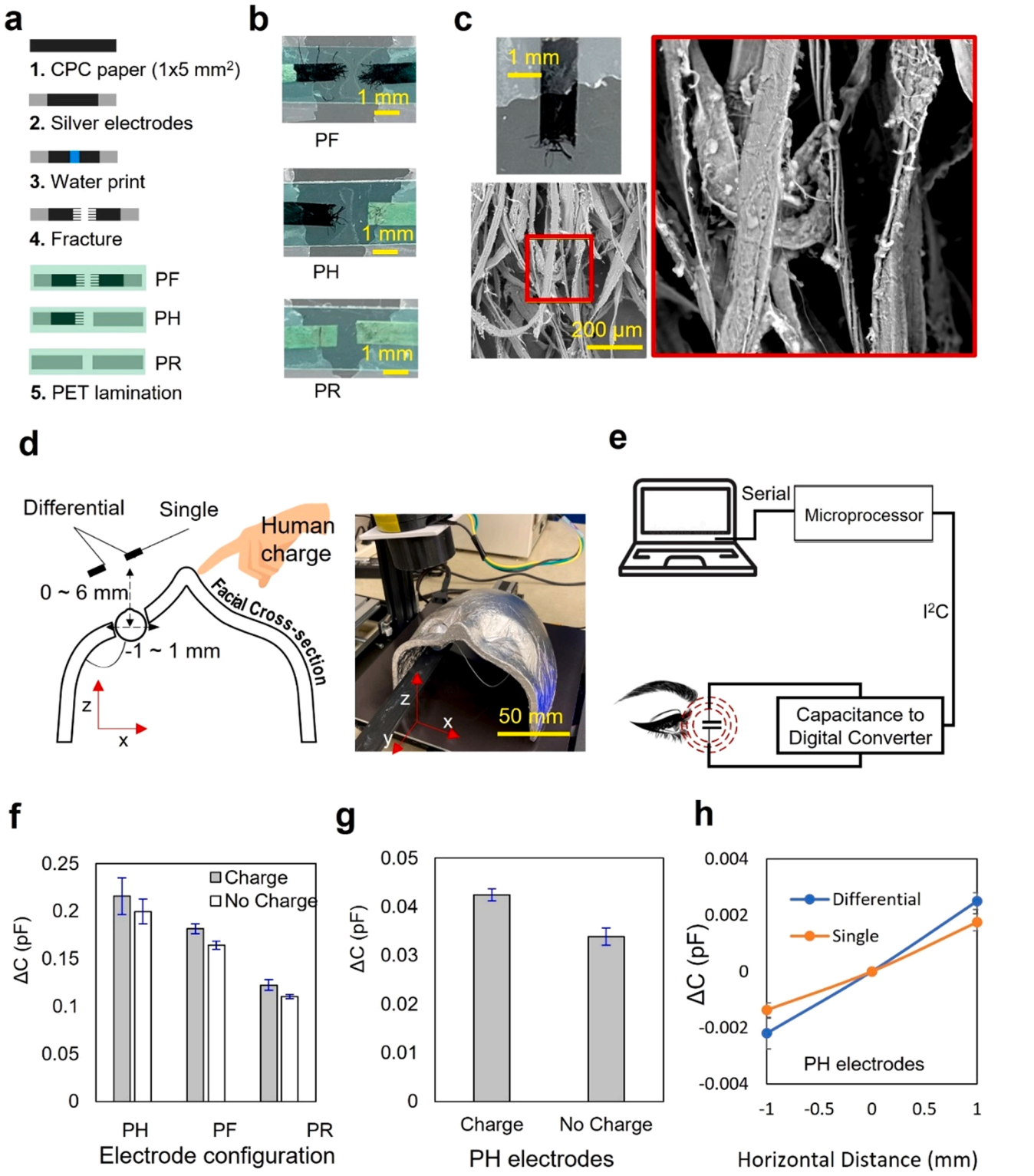

Fig. 2. Sensor fabrication and characterization. (a) Sensor fabrication process and fabricated sensors. **(b)** Fibrous, hybrid, and rectangular sensors. **(c)** Optical and SEM images of a representative fibrous electrode. **(d)** An eye and a face simulator covered with a conductive aluminum foil. **(e)** Capacitance measurement configuration using a capacitance-to-digital chip. **(f)** ΔC for hybrid, fibrous, and rectangular sensors for 0–6 mm displacement between a face and eyeball (N = 3). ΔC is measured with and without human charge. **(g)** ΔC for a hybrid sensor with the displacement of an eyeball without moving a face (ΔC for 0–6 mm distance) (N = 3). The sensor is initially located at 0 mm from the sensor. **(h)** Comparison of ΔC for single- and differential capacitive measurement for ± 1 mm horizontal movement of an eyeball at the distance of 6 mm to a sensor (N = 3).

resolution of 0.5 fF. FDC1004 was capable of four single or two pairs of differential sensors, with a sampling rate of 100 Hz/sensor. This allowed for monitoring horizontal and vertical eye movement over 60 Hz, which was the standard for camera-based eye trackers.

3.1.2. Sensor characterization using a face simulator

The response of the fabricated capacitive sensors was analyzed by using a face simulator according to the sensor configurations, geometry, and electric charge of a human face model with an eyeball. The human face model was 3D-printed using a polylactic acid (PLA) (Fig. 2d). The face and eyeball were covered with conductive aluminum foil and connected via a copper wire. The eyeball was placed on an x-y-z control stage to simulate human eye movement. The facial model and eyeball were located on an x-y plane, with stepper motor control along the z-axis. The body charge was applied to the facial model via a copper wire attached to the human hand. Capacitive sensors were placed at the bottom of a 3D printed PLA puck, which was tilted at 10 degrees to match the contour of the facial model and directed towards the eyeball. Sensors were connected to a capacitance-to-digital chip and a microprocessor. The face model had the geometry of a human face with an independent actuation of the eyeball and the nearby sensor. Fig. 2e shows the electric measurement configuration.

Using the setup, the sensitivity of the capacitive sensors was characterized for various facial conditions. In test 1, PR, PF, and PH sensors were displaced by 6 mm from the face fixed with an eyeball to characterize the sensitivity depending on the facial shape and body charge. Test 2 was conducted to evaluate the most sensitive PH sensor only when the eyeball was displaced 0–6 mm from the face. This test could also provide ΔC depending on the charge induced by the eyeball. The goal of test 3 was to compare single sensor configuration to differential sensors for ± 1 mm-horizontal eye movement at a 6 mm-distance. This test aimed to emulate a portion of actual eyeball movement during smooth pursuit. Tests 2 and 3 were performed with 1 mm-wide PH sensors, with and without body charge.

3.1.3. Capacitive measurement of human eye movement for sensor location optimization

The most sensitive PH sensor was used to track the motion of human eyes. A vertical eye movement test protocol was devised to evaluate sensor performance, whereby a human subject gazed at markers to rotate the eye vertically ± 20°. To calibrate vertical eye movements, a whiteboard was placed 680 mm away from the user's eyes and marked with two points, 248 mm above and below the neutral gaze position. Moving the gaze between these two markers was equal to a vertical angular rotation of ± 20°. Eye gazing was restricted to vertical movement, negating any diagonal or circular pathways. The eye movement process for vertical tests was as follows; three repetitions of vertical movement between the ± 20° markers, three repetitions of 0 ~ 20° from neutral location, and two repetitions of 0 ~ − 20° from neutral position. Movement time between markers was 1 s, with a hold time of 3 s at each marker. The eye displacement test was used to characterize the sensors, with respect to position, ΔC, and sensitivity.

For horizontal eye movement, differential capacitive measurement was conducted to study the optimal sensor locations. The same experimental setup was used but the gaze moved between two markers located ± 35° from the central position. The subject made alternating left- and right 70° horizontal eye movements between the two markers. A single human subject was used during sensor optimization trials.

3.1.4. Comparison test to a commercial eye tracker

The capacitive sensor signals of vertical and horizontal eye movements were compared to the eye tracking outputs of a video-based commercial eye tracker (Tobii Pro Nano). The commercial system captured gaze data at 60 Hz using a video-based pupil and corneal reflection eye tracking system with dark and bright pupil illumination modes. This eye tracker was designed for fixation-based studies after user calibration. The capacitive eye tracker's signal was compared to that of the commercial eye tracker in terms of motion accuracy and response time.

Supplementary material related to this article can be found online at doi:10.1016/j.sna.2022.113739.

The capacitive eye tracker was assembled with one pair of differential sensors for horizontal eye tracking, together with a single sensor for vertical eye movement detection using FDC1004. The data were recorded at the sampling rate of 45 Hz. The time-dependent capacitive data showed horizontal and vertical movement by differential- and single measurements, respectively. The test was conducted on three different human subjects. Due to the limitations of the commercial system, vertical and horizontal angular displacements were set to ± 9° and ± 16°, respectively. The degree of angular displacement was determined by the monitor size (diagonal distance: 685 mm) of a commercial eye tracker and the distance from the monitor to the human subject's face (788 mm). The corresponding data for a commercial eye tracker were unity displacement for horizontal and vertical movement. All tests were conducted indoors at room temperature. All study related to the capacitive eye tracking and the comparison test to the commercial eye tracker was approved by the institutional review board (IRB) at the University of Washington (IRB ID: STUDY00010741).

4. Results

4.1. Capacitive response to a face simulator

The presence of the human facial shape and charge profoundly affected the ΔC of the capacitive sensors. Fig. 2f compares ΔC of PH, PF, and PR sensors for the 0–6 mm-displacement between the sensors and the face with an eyeball with and without human charge. The starting position of 0 mm did not include a 50 μm-thick PET film thickness that covered sensors. In the comparison, the PH sensors showed the largest ΔC of 0.224 pF and 0.200 pF with and without a human charge, respectively. A PF sensor showed ΔC of 0.175 pF and 0.160 pF with and without a human charge, respectively. The PR sensor showed the smallest ΔC. These experimental data qualitatively agreed with the results of the numerical analysis.

Fig. 2g displays ΔC of PH sensors with and without body charge when an eyeball was moved from 0 m to 6 mm from the face (N = 3). A PH sensor showed only ΔC= 42 fF with the human charge. In comparison to the experiment moving a PH sensor from the entire face in Fig. 2f, ΔC was only 18.7%. Although the human charge contributed to increasing ΔC, the isolated eye movement with the background of the whole face showed only limited ΔC. Considering 6 mm-displacement, the actual ΔC for human eye movement could be further reduced.

Besides the out-of-plane displacement, a human eye could move horizontally from a sensor. When single capacitive measurement was conducted for 1 mm-horizontal movement at 6 mm proximity of a sensor, the ΔC was only 1.7 fF (Fig. 2h). The differential capacitive measurement increased ΔC by 55%. Therefore, differential capacitive measurement increased ΔC and, thus, sensitivity.

4.2. Capacitive response to human eye movement

4.2.1. Vertical eye movement

For vertical eye movement, a single capacitive measurement was conducted to study the optimal sensor location. In Fig. 3a, the locations of a sensor are presented. For vertical movement, the sensor locations were tested from (0, 20) to (0, −25) by varying the vertical position in − 5 mm increments. The origin of the coordinate represents the center point of the cornea. The x-y coordinates correspond to the x-y plane of the glasses shown in Fig. 1a. Vertical and horizontal eye movement was conducted according to the designed protocol by watching the spots on a whiteboard (Fig. 3b). For vertical eye movement, only a single measurement was conducted because differential capacitive measurement

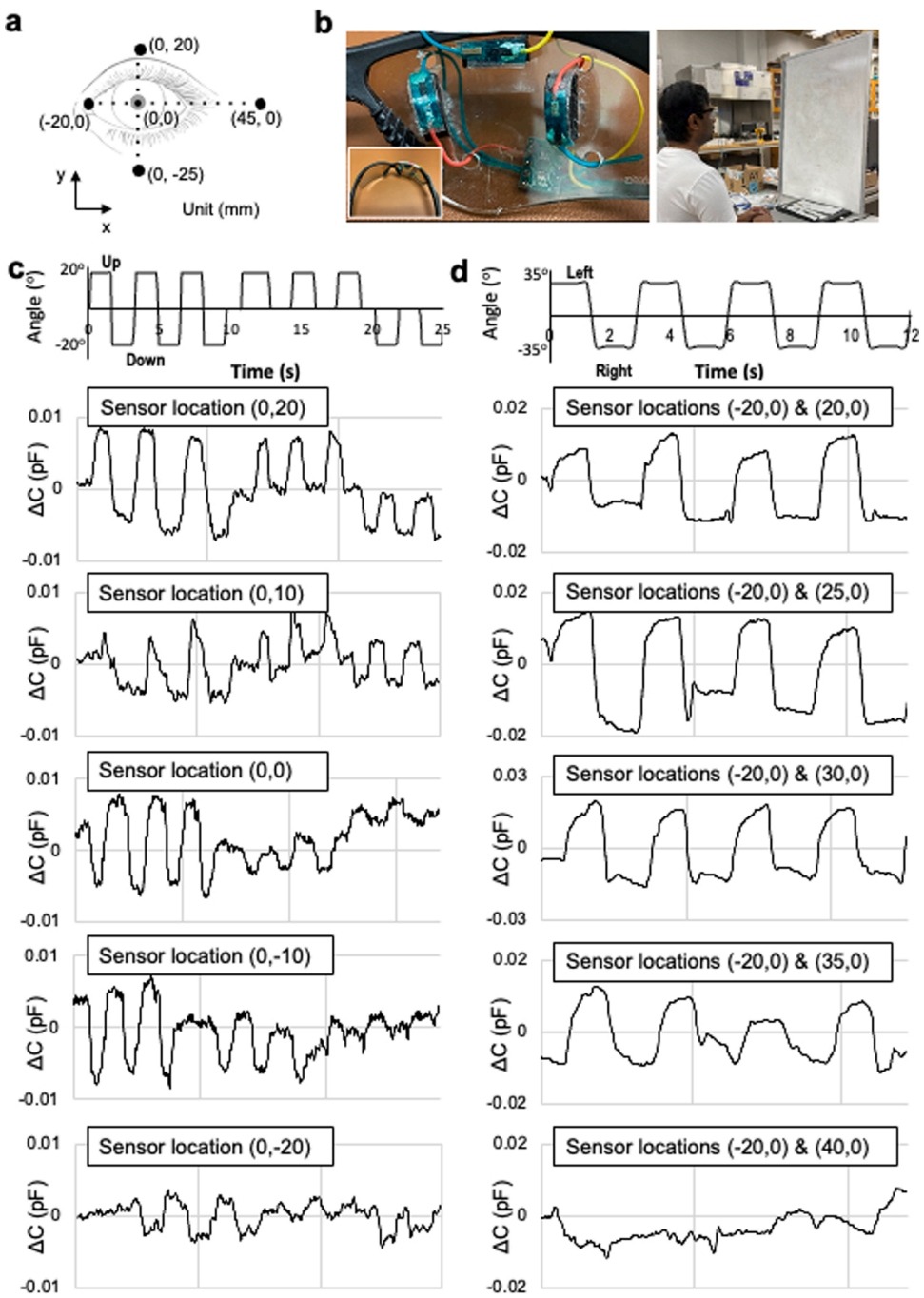

Fig. 3. Vertical and horizontal eye movement tests. (a) Locations of sensors for single and differential capacitive measurement. **(b)** Monocular eyeglasses installed with single vertical and differential horizontal sensors. **(c)** ΔC depending on vertical sensor locations at (0, 20), (0, 10), (0, 0), (0, −10), and (0, −20). **(d)** ΔC depending on horizontal differential sensor locations at [(−20, 0) and (20, 0)], [(−20, 0) and (25, 0)], [(−20, 0) and (30, 0)], [(−20, 0) and (35, 0)], and [(−20, 0) and (40, 0)].

showed undesirable patterns (Supplementary Information, Fig. S8). While vertical movements were measured by single capacitance, horizontal differential sensors were also sensitive to the vertical movements. With the increased sensitivity of differential capacitance, the change in proximity of the cornea and eyelid to the differential sensors during vertical movement led to detection of this movement as a sinusoidal pattern. As such, a single vertical measurement was used to reduce sensitivity to horizontal eye movements while, enabling sensitivity towards only vertical eye movements.

The time-dependent protocol of eye movement in the top graph of Fig. 3c showed vertical displacement of ± 20°. The sensor location of (0, 20) clearly showed the reproducible measurement of eye movements and identified the straight neutral gaze at the midline (Fig. 3c). At the sensor location of (0, 0), the phase of ΔC started to be inverted. As the sensor moved to (0, −10) and (0, −20), ΔC was inverted in comparison to that of (0, 20), as the sensors at these locations were inversely influenced by the eye. Moreover, the amplitude decreased as the sensor location was below (0, 0). At location (0, −25), the sensor produced inconsistent amplitude and distortion.

It was speculated that the capacitive signal for vertical eye movement was dominated by cornea movement rather than eyelid movement. To evaluate the source of the capacitive signal, photographic angular analysis (Supporting Information, Fig. S9a) of the eye was conducted. A frame-by-frame photo analysis was undertaken to determine the displacement of the cornea and eyelid during vertical eye movement, with respect to sensor position (Supporting information, Fig. S9b). From the initial distance of 6 mm, the cornea diagonally retracted by 7.1 mm as the eye gazed between 20 to − 20°. A diagonal retraction of 7.1 mm equated to ~2 mm of corneal retraction in the x plane (refer to Supporting Information, Fig. S9a). In comparison, the eyelid was located at

– 1 mm at 20° and withdrawn by 3 mm at – 20°. This data confirmed the complex movement relationship between the cornea and eyelid, where the photographic displacement could not individually explain the relationship between the capacitance signal and gaze position.

As such, the capacitance effect of the eyelid encasing the cornea was also examined. As the eyelid moved from nearly closed- to fully closed state, a sharp spike rose in capacitance (Supporting Information, Fig. S9c). The dielectric nature and electric charge of the cornea and eyelid could dominate ΔC. To mimic the capacitance interaction between a wet eyeball and dry eyelid, when a sensor moved between wet and dry skin, the ΔC was much greater on the wet skin (Supporting Information, Fig. S9d). On average, the wet skin exhibited ΔC of 24 fF, greater than that of the dry skin. The larger ΔC could be caused by direct electrical connection to the human body charge and the electrical double layer forming on the skin.

According to the results, the cornea with the thin water layer could dominate ΔC until the eyelid was completely closed. The inversion and decreased amplitude of ΔC at the vertical sensor locations (0, 0) and below could be explained with respect to cornea and eyelid protuberance. The signal was inverted at sensor locations (0, 0) and below as the cornea was at a closer proximity to the sensor during its downward trajectory. The amplitude decreased, as less of the cornea was interacting with the sensor. Further study is required to quantify the impact of the eyelid on ΔC. In summary, the sensor location between (0, 20) and (0, 10) was optimal with a maximum range of ± 10 fF. Considering the noise level of 0.56 fF_{RMS} and sensitivity of 0.5 fF/deg, the accuracy was 1.1 degrees.

4.2.2. *Capacitive response to horizontal eye movement*

For horizontal eye movement, differential capacitive measurement

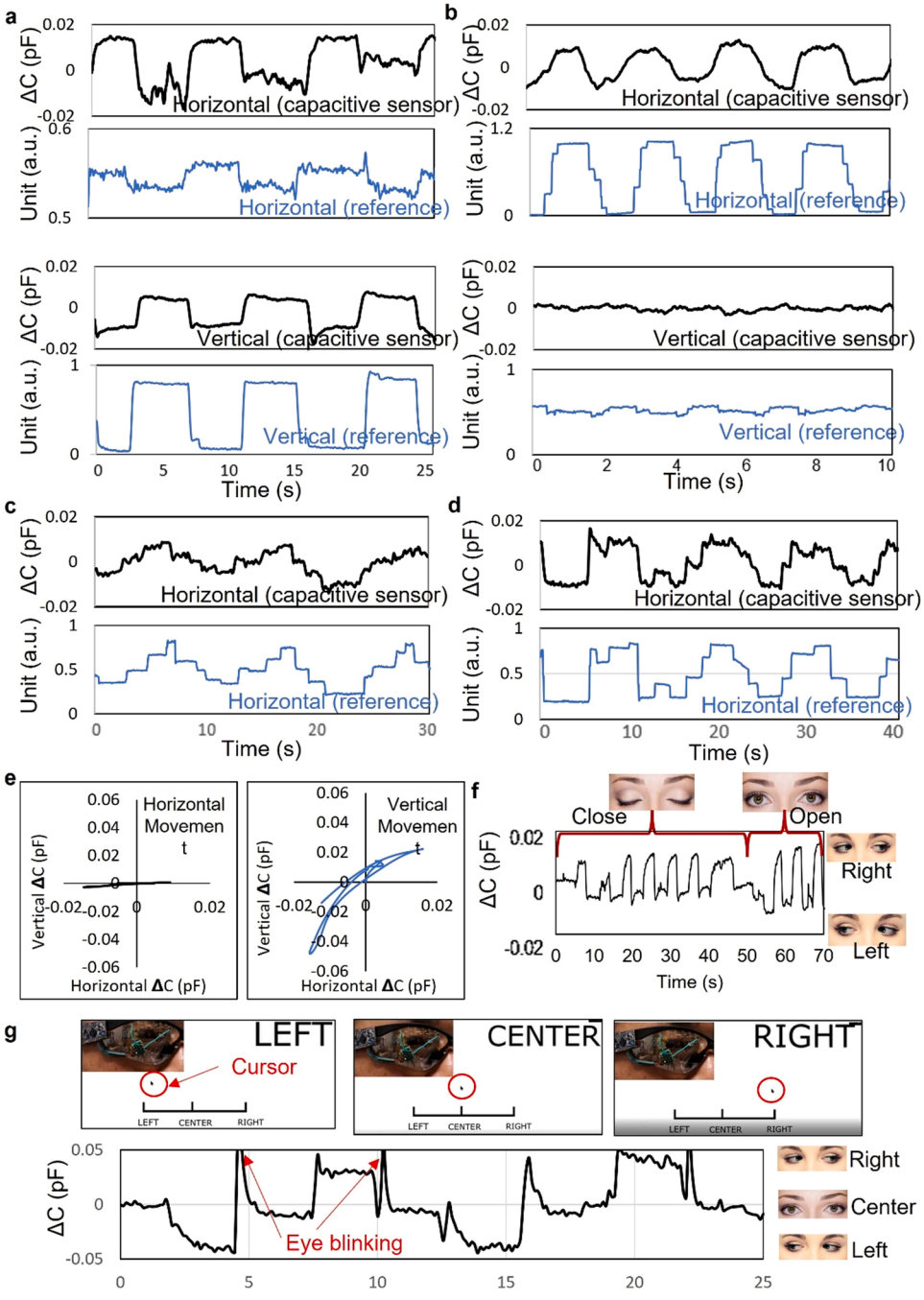

Fig. 4. Comparison to a commercial eye tracker and other applications (a) Comparison of a capacitive eye tracker to a commercial eye tracker for vertical eye movement. **(b)** Comparison of a capacitive eye tracker to a commercial eye tracker for horizontal eye movement. **(c)** Comparison of a capacitive eye tracker to a commercial eye tracker for horizontal eye movement. **(d)** Comparison of a capacitive eye tracker to a commercial eye tracker for horizontal eye movement. **(e)** Phase diagrams for horizontal and vertical smooth pursuit movements shown. **(f)** ΔC of closed and open eyes for horizontal movement. **(g)** Human-machine interface for horizontal eye movement. Eyes are controlled at the left, center, and right locations (Supporting Information, video clip).

was chosen to study the optimal sensor locations. The same experimental protocol was used, but the gaze moved between two targets located at − 35° (left) and + 35° (right). The subjects repeated the 70° gaze shift four times (Fig. 3d). The horizontal eye movement excursion was limited by the subject's oculomotor range. Single capacitive measurement was not used due to the low sensitivity.

Both sensors in the differential configuration were placed on the left and right sides of the right eye. The design of the glass frame only allowed the left sensor to be placed at (−20, 0) near the nose bridge. The location of the right-side sensor was tested between (20, 0) and (40, 0) in 5 mm increments to find the optimal sensors' location. The midline of the waveform corresponded to a straight neutral gaze.

When the right sensor was located between (20, 0) and (30, 0), the capacitive signals clearly showed rightward, leftward, and zero-crossing movements. Moreover, the signals showed consistent movement amplitudes. At location (35, 0), the signal reduced amplitudes. At the most peripheral location (40, 0), the sensor failed to produce a predictable signal. The failure was caused by the lack of sensitivity from the right sensor because the sensor was located beyond the eye corner. Differential sensors located at [(−20, 0) & (20, 0)] and [(−20, 0) & (30, 0)] were optimal with a maximum range of ± 10 fF and sensitivity of 0.28 fF/deg. With a noise level of 0.35 fF_{RMS}, the accuracy was within 0.8 degrees.

4.3. Comparison test to a commercial eye tracker

The capacitive sensor signals of vertical and horizontal eye movements were compared with those produced by a camera-based commercial eye tracker (Tobii Pro Nano). Section 3.5 describes the experimental setup for the comparison test using a commercial eye tracker. Fig. 4a shows the vertical movement of an eyeball. As the eye moved vertically, both the vertical and horizontal ΔC clearly showed the movement signals with similar amplitudes and opposite phases. The commercial eye tracker also produced eye movement signals in both the vertical and horizontal channels during a pure vertical eye movement, but the amplitude of the horizontal signal was ~3% of the vertical signal.

Fig. 4b shows the comparisons of horizontal eye movement signals produced by the capacitive sensors and the Tobii eye tracker. In contrast to vertical eye movement, the horizontal ΔC showed a robust horizontal movement signal, but the vertical ΔC did not show any signals related to the horizontal eye movement. Based on the results, the vertical capacitive sensor determined the movement direction of an eyeball. Based on the results shown in Fig. 4a and b, combining both amplitude and phase information from both vertical and horizontal capacitive sensors allowed for horizontal and vertical signal separation due to the crosstalk during vertical eye movement.

Fig. 4c and d show the comparison of horizontal eye movement signals between capacitive sensors and a commercial eye tracker for two other human subjects. The capacitive sensors clearly detected the saccades. In comparison to the ΔC shown in Fig. 4b (top panel), the saccadic eye movements were more distinctly shown and clearly correlated to those produced by a commercial eye tracker. Overall, ΔC ranged between 10 and 20 fF. Considering horizontal eye movements of ± 12°, 1° accuracy could be achieved for horizontal eye movement.

Fig. 4e depicts the phase diagrams for vertical and horizontal smooth pursuit movement, for qualitative deduction of the direction of eye movement. During horizontal smooth pursuit, the phase diagram produced a plot with negligible vertical amplitude. However, during vertical smooth pursuit, the phase diagram produced a diagonal plot. A clear qualitative distinction was evident between the phase diagrams.

5. Discussion

For a capacitive eye tracker, the performance of a high accuracy capacitance-to-digital chip was crucial for accurate detection of eye movement. In our tests, various chips were tested, including AD7747 (Analog Devices), FDC1004 (Texas instrument), and FDC2214 (Texas instrument). Also, LM 555 timer (Texas instrument) could be used for capacitive eye tracking. According to our characterization, 0.1 fF of accuracy was critical to obtain 1°-accuracy for eye movement. In this regard, AD7747 was the best in terms of accuracy. Despite the lower 1 fF-accuracy of FDC 1004, the higher sampling rate up to 400 Hz could be useful for ultimate eye tracking. FDC 2214 was an electrical resonance circuit with operation frequency of 1–3 MHz. Due to the resonance, the ΔC was high with the increased noise level. The sampling rate of FDC 2214 could be increased to 1 kHz, which had a potential for eye tracking.

The capacitive eye tracker was also tested to monitor horizontal eye movement with the eyelids closed and opened (Fig. 4f). The capacitive sensors reliably detected eye movement in both conditions. The amplitudes were larger when the eyelids opened. The ability of the sensors to detect eye movement with the closed eyelids would allow the sensors to be used in sleep studies.

To demonstrate the real-time response for detecting eye movement, the capacitive sensing eye tracker was interfaced with a laptop computer to control a cursor on the screen (Fig. 4g). Starting from a center point, the eyes moved to the left, center, and right locations according to verbal signals. The cursor showed corresponding movements to the three locations. Eye blinking (Fig. 4g, red arrows) showed spikes but did not appear to affect the accuracy of the cursor placements (Supporting Information, Real eye tracking HMI.mp4). The wearable eye tracker demonstrated the capability to control a machine using eyeball movement.

6. Conclusion

A capacitive eye tracker was demonstrated to monitor eye movement. Based on our numerical analysis, a hybrid capacitive sensor made of fibrous and rectangular electrodes had the highest sensitivity due to the reduced initial capacitance and increased capacitance change (ΔC) in the presence of an eyeball. In comparison to a single sensor, a differential sensor configuration showed the better detection performance. In the study using a face model, the human charge increased ΔC, but the face background reduced ΔC of eye movement. In the human subject test, the single capacitive measurement was optimal for vertical eye movement at the locations of (0, 20) ~ (0, 10) mm. For horizontal eye movement, the differential capacitive methods allowed accurate measurement at the locations between [(−20, 0) & (20, 0)] and [(−20, 0) & (30, 0)]. The accuracies for vertical and horizontal movement were 1.1 and 0.8 degrees, respectively. The comparison of a capacitive eye tracker to a commercial eye tracker showed a good correlation for horizontal- and vertical eye movements. A phase diagram between vertical and horizontal signals was used to qualitatively assess eye movement. The presented capacitive eye tracker detected horizontal eye movement with the closed and open eyelids. The relationship between cornea and eyelid position was studied to understand their consequence on the capacitance signal. The cornea was found to dominate the capacitance signal, until the eyelid was fully closed. The presented wearable capacitive eye tracker shows potential for eye tracking in various fields, including neuroscience, cognitive science, eye function diagnosis, and entertainment.

CRediT authorship contribution statement

Vigneshwar Sakthivelpathi: Conceptualization, Methodology, Software, Investigation, Formal analysis, Data curation, Writing, Visualization. **Zhongjie Qian:** Methodology, Software, Formal analysis, Data curation, Validation, Resources. **Tianyi Li:** Data analysis and Sensing Mechanism Analysis. **Sanggyeun Ahn**: Conceptualization, Methodology, Design. **Anthony B. Dichiara:** Resources, Writing, Funding acquisition. **Robijanto Soetedjo:** Methodology, Formal

analysis, Resources, Writing, Funding acquisition. **Jae-Hyun Chung:** Conceptualization, Methodology, Formal analysis, Validation, Resources, Writing, Supervision, Project administration, Funding acquisition.

Declaration of Competing Interest

The authors declare that they have no known competing financial interests or personal relationships that could have appeared to influence the work reported in this paper.

Data availability

Data will be made available on request.

Acknowledgements

VS, TL, RS and JC acknowledge the partial support from the National Eye Institute of NIH (R21 EY031768). VS, ZQ, ABD, JC acknowledge the partial support from the Advanced Manufacturing Program of National Science Foundation (No. 1927623). The authors acknowledge the partial support from IP group and Somalytics fund.

Appendix A. Supporting information

Supplementary data associated with this article can be found in the online version at doi:10.1016/j.sna.2022.113739.

References

[1] R.G. Alexander, S.L. Macknik, S. Martinez-Conde, Microsaccade characteristics in neurological and ophthalmic disease, Front Neurol. 9 (144) (2018) 1–9.
[2] M.R. MacAskill, T.J. Anderson, Eye movements in neurodegenerative diseases, Curr. Opin. Neurol. 29 (1) (2016) 61–68.
[3] R.P. Balandong, et al., A review on EEG-based automatic sleepiness detection systems for driver, IEEE Access 6 (2018) 22908–22919.
[4] Q. Ran, et al., Abnormal amplitude of low-frequency fluctuations associated with rapid-eye movement in chronic primary insomnia patients, Oncotarget 8 (49) (2017) 84877–84888.
[5] M.I. Posner, C.R. Snyder, B.J. Davidson, Attention and the detection of signals, J. Exp. Psychol. Gen. 109 (2) (1980) 160–174.
[6] T. Van Gog, K. Scheiter, A eye tracking as a tool to study and enhance multimedia learning, Learn Instr. 20 (2) (2010) 95–99.
[7] T. Usui, et al., Night blindness with depolarizing pattern of on/off response in electroretinogram: A case report, Doc. Ophthalmol. 111 (1) (2005) 15–21.
[8] S. Montagnese, P. Amodio, M.Y. Morgan, Methods for diagnosing hepatic encephalopathy in patients with cirrhosis: A multidimensional approach, Metab. Brain Dis. 19 (3–4) (2004) 281–312.
[9] A. Paolozza, et al., Diffusion tensor imaging of white matter and correlates to eye movement control and psychometric testing in children with prenatal alcohol exposure, Hum. Brain Mapp. 38 (1) (2017) 444–456.
[10] M.P. Grant, et al., Abnormal eye movements in Creutzfeldt-Jakob disease, Ann. Neurol. 34 (2) (1993) 192–197.
[11] U. Rosenhall, E. Johansson, C. Gillberg, Oculomotor findings in autistic children, J. Laryngol. Otol. 102 (5) (1988) 435–439.
[12] G.M. Jones, J.D. DeJong, Dynamic characteristics of saccadic eye movements in Parkinson's disease, Exp. Neurol. 31 (1) (1971) 17–31.
[13] G. Avanzini, et al., Oculomotor disorders in Huntington's chorea, J. Neurol. Neurosurg. Psychiatry 42 (7) (1979) 581–589.
[14] A.F. Fuchs, C.R. Kaneko, C.A. Scudder, Brainstem control of saccadic eye movements, Annu Rev. Neurosci. 8 (1985) 307–337.
[15] E.L. Keller, N.J. Gandhi, J.M. Shieh, Endpoint accuracy in saccades interrupted by stimulation in the omnipause region in monkey, Vis. Neurosci. 13 (6) (1996) 1059–1067.
[16] E.L. Keller, N.J. Gandhi, Vijay, S. Sekaran, Activity in deep intermediate layer collicular neurons during interrupted saccades, Exp. Brain Res. 130 (2) (2000) 227–237.
[17] W. Becker, The neurobiology of saccadic eye movements, Metrics. Revs Oculomot. Res. 3 (1989) 13–67.
[18] A. Galvan, et al., Nonhuman primate optogenetics: recent advances and future directions, J. Neurosci. 37 (45) (2017) 10894–10903.
[19] L. Grosenick, J.H. Marshel, K. Deisseroth, Closed-loop and activity-guided optogenetic control, Neuron 86 (1) (2015) 106–139.
[20] Y. El-Shamayleh, et al., Selective optogenetic control of purkinje cells in monkey cerebellum, Neuron 95 (1) (2017) 51–62.
[21] D.A. Robinson, A method of measuring eye movement using a scleral search coil in a magnetic field, IEEE Trans. Bio-Med. Eng. 10 (4) (1963) 137–145.
[22] A.F. Fuchs, D.A. Robinson, A method for measuring horizontal and vertical eye movement chronically in the monkey, J. Appl. Physiol. 21 (3) (1966) 1068–1070.
[23] S.J. Judge, B.J. Richmond, F.C. Chu, Implantation of magnetic search coils for measurement of eye position: An improved method, Vis. Res. 20 (6) (1980) 535–538.
[24] M.M. Houben, J. Goumans, J. van der Steen, Recording three-dimensional eye movements: Scleral search coils versus video oculography, Invest Ophth Vis. Sci. 47 (1) (2006) 179–187.
[25] O.V. Acuna, P. Aqueveque, E.J. Pino, Eye-tracking capabilities of low-cost EOG system, Eng. Med Biol. Soc. Ann. 2014 (2014) 610–613.
[26] Y. Jia, C.W. Tyler, Measurement of saccadic eye movements by electrooculography for simultaneous EEG recording, Behav. Res Methods 51 (5) (2019) 2139–2151.
[27] A.J. Golparvar, M.K. Yapici, Toward graphene textiles in wearable eye tracking systems for human-machine interaction, Beilstein J. Nanotechnol. 12 (2021) 180–189.
[28] S. Lee, et al., Ultrathin nanogenerators as self-powered/active skin sensors for tracking eye ball motion, Adv. Funct. Mater. 24 (8) (2014) 1163–1168.
[29] N.I. Kim, et al., Highly-sensitive skin-attachable eye-movement sensor using flexible nonhazardous piezoelectric thin film, Adv. Funct. Mater. 31 (8) (2021), 2008242-1-11.
[30] Moller C., Ribeiro F.P. Capacitive sensors for determining eye gaze direction. US9888843B2 (Patent). 2018.
[31] D.W. Hansen, Q. Ji, In the eye of the beholder: a survey of models for eyes and gaze, IEEE T Pattern Anal. 32 (3) (2010) 478–500.
[32] A.B. Dichiara, et al., Smart papers comprising carbon nanotubes and cellulose microfibers for multifunctional sensing applications, J. Mater. Chem. A. 5 (38) (2017) 20161–20169.
[33] J.Y. Zhang, et al., Electromechanical coupling of isotropic fibrous networks with tailored auxetic behavior induced by water-printing under tension, J. Mater. Chem. C. 9 (13) (2021) 4544–4553.
[34] A.E. Zavadskii, X-ray diffraction method of determining the degree of crystallinity of cellulose materials of different anisotropy, Fibre Chem. 36 (2004) 425–430.
[35] S. Goodman, et al., Scalable manufacturing of fibrous nanocomposites for multifunctional liquid sensing, Nano Today 40 (2021), 101270.
[36] S. Bi, et al., Ultrasensitive and highly repeatable pen ink decorated cuprammonium rayon (cupra) fabrics for multifunctional sensors, J. Mater. Chem. A 6 (2018) 16556–16565.

Vigneshwar Sakthivelpathi is a Graduate Student in the Ph.D. program, in the Department of Mechanical Engineering at the University of Washington.

Zhongjie Qian is a Graduate Student in the Ph.D. program, in the Department of Mechanical Engineering at the University of Washington.

Tianyi Li is a Graduate Student in the Ph.D. program, in the Department of Mechanical Engineering at the University of Washington.

Sanggyeun Ahn is an Associate Professor in the School of Art, Art History and Design at the University of Washington. Ahn's research interest includes human factor study, biomedical device design, and industrial design.

Anthony B. Dichiara is an Assistant Professor in the School of Environmental and Forest Sciences' Bioresource Science and Engineering at University of Washington. Dichiara's research investigates the synthesis of nanomaterials from biomass; characterization of biomaterials and their applications in multifunctional composites and environmental remediation.

Robijanto Soetedjo is a Neurophysiologist and Research Assistant Professor in the Department of Physiology and Biophysics at the University of Washington. Soetedjo's areas of interest includes systems neuroscience and motor control learning. Soetedjo's research investigates the neural mechanism of saccade generation and the mechanisms underlying saccade adaptive capability.

Jae-Hyun Chung is an Associate Professor in the Department of Mechanical Engineering at University of Washington. Chung's research interests include micro/nanoscale fabrication, carbon nanotube-based sensors, point-of-care (POC) medical devices, and wearable sensors.